

Electronic structure and spectral properties of Am, Cm and Bk: Charge density self-consistent LDA+HIA calculations in FP-LAPW basis

A. B. Shick¹, J. Kolorenč^{1,2}

¹*Institute of Physics, ASCR, Na Slovance 2, CZ-18221 Prague, Czech Republic and*

²*Department of Physics and CHiPS, North Carolina State University, Raleigh, North Carolina 27695, USA*

A. I. Lichtenstein

University of Hamburg, Jungiusstrasse 9, 20355 Hamburg, Germany

L. Havela

*Department of Condensed Matter Physics, Faculty of Mathematics
and Physics, Charles University, Prague, Czech Republic*

(Dated: November 3, 2018)

We provide a straightforward and numerically efficient procedure to perform local density approximation + Hubbard I (LDA+HIA) calculations, including self-consistency over the charge density, within the full potential linearized augmented plane wave (FP-LAPW) method. This implementation is all-electron, includes spin-orbit interaction, and makes no shape approximations for the charge density. The method is applied to calculate selected heavy actinides in the paramagnetic phase. The electronic structure and spectral properties of Am and Cm metals obtained are in agreement with previous dynamical mean-field theory (LDA+DMFT) calculations and with available experimental data. We point out that the charge density self-consistent LDA+HIA calculations predict the f charge on Bk to exceed the atomic integer f^8 value by 0.22.

PACS numbers: 71.27.+a,79.60.-i

I. INTRODUCTION

It is known that conventional band theory—local density approximation (LDA) and its semi-local extension, generalized gradient approximation (GGA)—gives poor results for actinides. Since the LDA/GGA results are qualitatively incorrect already at the level of ground state properties, like the equilibrium volume and magnetization, the electronic structure theory of actinides requires that electron-electron correlations are included beyond those given by conventional LDA/GGA. Lately, several correlated band theory approaches have been put forward: LDA+Hubbard U (LDA+U) [1, 2], the hybrid functional (HYF) approach [3] or the self-interaction-corrected local spin-density (SIC-LSD) [4]. Each of them achieved an improvement of some particular aspects of the electronic structure of actinides.

None of these correlated band theories has been capable to correctly describe spectral properties of actinides. Recently, the excitations in Pu and Am were extensively studied with the aid of a combination of the LDA and the dynamical mean-field theory (LDA+DMFT) [5, 6, 7, 8, 9], that successfully explains the experimentally observed multi-peak structure in Pu valence-band photoelectron spectra (PES). In spite of obvious progress in the LDA+DMFT theory, it has been mostly focused on calculations of excitations and implemented on the basis of a tight-binding Hamiltonian built from the LDA, without self-consistency over the charge den-

sity.

In this paper we present a simple and numerically efficient procedure to combine the LDA+Hubbard I approximation (HIA), including self-consistency over the charge density, with the full potential linearized augmented plane wave (FP-LAPW) method [10]. The FP-LAPW method makes no shape approximation for the charge density and is considered to be state-of-the-art in accuracy. We apply our implementation to the electronic structure and spectroscopic properties of heavy actinides: Am, Cm and Bk.

There is a revival of interest to the electronic and spectroscopic properties of heavy actinides [11]. Superconducting temperature of Am shows complex and unconventional dependence on lattice structure transformations [12]. On the basis of standard band structure calculations it was proposed that curium is one of a few elements that has its lattice structure stabilized by magnetism [13]. The spectroscopic studies [14] suggested that $5f$ states of Cm are shifted towards the LS coupling limit, unlike most actinide elements where the intermediate coupling prevails.

The paper is organized as follows. For the sake of completeness, in Sec. II we recall the basic equations of the LDA+DMFT in a formulation of Ref. [15]. Then we describe charge density self-consistent LDA+HIA approximation implemented in FP-LAPW method. In Sec. III we present the results of the charge density self-consistent LDA+HIA calculations for $5f$ Am, Cm, and Bk elemental met-

als in the paramagnetic state. These results are compared with previous work and additional features are pointed out.

II. METHODOLOGY

We start with the multi-band Hubbard Hamiltonian [15] $H = H^0 + H^{\text{int}}$, where

$$\begin{aligned} H^0 &= \sum_{i,j} \sum_{\gamma_1, \gamma_2} H_{i\gamma_1, j\gamma_2}^0 c_{i\gamma_1}^\dagger c_{j\gamma_2} \\ &= \sum_{\mathbf{k}} \sum_{\gamma_1, \gamma_2} H_{\gamma_1, \gamma_2}^0(\mathbf{k}) c_{\gamma_1}^\dagger(\mathbf{k}) c_{\gamma_2}(\mathbf{k}) \end{aligned} \quad (1)$$

is the one-particle Hamiltonian found from ab initio electronic structure calculations of a periodic crystal, including the spin-orbit coupling (SOC). The indices i, j label lattice sites, $\gamma = (lm\sigma)$ denote spinorbitals $\{\phi_\gamma\}$, and \mathbf{k} is a k-vector from the first Brillouin zone. It is assumed that the electron-electron correlations between s , p , and d electrons are well described within the density functional theory, while the correlations between the f electrons have to be considered separately by introducing the interaction Hamiltonian

$$\begin{aligned} H^{\text{int}} &= \frac{1}{2} \sum_i \sum_{m_1, m_2, m_3, m_4}^{\sigma, \sigma'} \langle m_1, m_2 | V_i^{ee} | m_3, m_4 \rangle \\ &\quad \times c_{im_1\sigma}^\dagger c_{im_2\sigma'}^\dagger c_{im_4\sigma'} c_{im_3\sigma}. \end{aligned} \quad (2)$$

The operator V^{ee} represents an effective on-site Coulomb interaction [15] expressed in terms of the Slater integrals F_k and the spherical harmonics $|lm\rangle$.

In what follows we use a local approximation for the one-particle selfenergy $\Sigma(\mathbf{k}, z)$ which contains the electron-electron correlations, i. e., we assume that the selfenergy is site-diagonal and therefore independent of \mathbf{k} . The corresponding one-particle Green function reads

$$G(\mathbf{k}, z) = \left(z + \mu - H^0(\mathbf{k}) - \Sigma(z) \right)^{-1}, \quad (3)$$

where z is a (complex) energy measured with respect to the chemical potential μ . The interaction term, Eq. (2), acts only in the subspace of f -states. Consequently, the selfenergy $\Sigma(z)$ is nonzero only in the subspace of the f -states.

The self-consistent procedure to solve the periodic lattice problem in the DMFT approximation is now formulated in the usual way making use of the ‘‘impurity’’ method of Ref. [15]. The DMFT self-consistency condition is achieved by equating the local Green function in a solid to the Green function of a single-impurity Anderson model (SIAM) that describes an isolated multiorbital impurity surrounded by a bath of uncorrelated delocalized electrons. Starting with the single-particle Hamiltonian

$H^0(\mathbf{k})$ and a guess for the local selfenergy $\Sigma(z)$, the local Green function is calculated by integrating $G(\mathbf{k}, z)$, Eq. (3), over the Brillouin zone. Subsequently, bath Green function (the so-called Weiss field) is calculated [15], and used to solve the SIAM. New local $\Sigma(z)$ is evaluated, which is inserted back into Eq. (3). In addition, the charge density needed to construct the single-particle Hamiltonian $H_0(\mathbf{k})$ in Eq. (3) has to be calculated self-consistently from the local Green function.

A. Hubbard-I approximation for $\Sigma(z)$

We make use of the multiorbital HIA, which is suitable for incorporating the multiplet transitions into the electronic structure, as it is explicitly based on the exact diagonalization of an isolated atomic-like shell. Further, we restrict our formulation to the paramagnetic phase. In HIA, only the site-diagonal terms from one-particle Hamiltonian Eq. (1) are retained [15], and the on-site atomic-like Hamiltonian including SOC is constructed, see also Ref. [7],

$$\begin{aligned} H^{\text{at}} &= \sum_{m_1, m_2}^{\sigma, \sigma'} \xi (\mathbf{1} \cdot \mathbf{s})_{m_1 m_2}^{\sigma \sigma'} c_{m_1 \sigma}^\dagger c_{m_2 \sigma'} \\ &\quad + \frac{1}{2} \sum_{m_1 \dots m_4}^{\sigma, \sigma'} \langle m_1 m_2 | V^{ee} | m_3 m_4 \rangle \\ &\quad \times c_{m_1 \sigma}^\dagger c_{m_2 \sigma'}^\dagger c_{m_4 \sigma'} c_{m_3 \sigma}, \end{aligned} \quad (4)$$

where ξ is the SOC parameter. Note that the crystal field terms are not included in Eq. (4), and will be treated on the LDA level that is sufficient for our applications.

Consecutively, exact diagonalization, $H^{\text{at}}|\nu\rangle = E_\nu|\nu\rangle$, is performed in order to obtain all eigenvalues E_ν and eigenvectors $|\nu\rangle$ that are used to calculate the atomic Green function

$$\begin{aligned} [G^{\text{at}}(z)]_{\gamma_1 \gamma_2} &= \frac{1}{Z} \sum_{\nu, \mu} \frac{\langle \mu | c_{\gamma_1} | \nu \rangle \langle \nu | c_{\gamma_2}^\dagger | \mu \rangle}{z + E_\mu - E_\nu + \mu_H} \\ &\quad \times \left[e^{-\beta(E_\nu - \mu_H N_\nu)} + e^{-\beta(E_\mu - \mu_H N_\mu)} \right]. \end{aligned} \quad (5)$$

Here β is the inverse temperature, Z is the partition function, and N_ν is the number of particles in the state $|\nu\rangle$. These N_ν are eigenvalues of the particle number operator that commutes with the atomic Hamiltonian Eq. (4). Parameter μ_H plays a role of the HIA chemical potential. Actual choice of μ_H will be discussed later. Finally, the atomic self-energy is evaluated as

$$\begin{aligned} \left[\Sigma_H(z) \right]_{\gamma_1 \gamma_2} &= z \delta_{\gamma_1 \gamma_2} \\ &\quad - \left[\xi (\mathbf{1} \cdot \mathbf{s}) + \left(G^{\text{at}}(z) \right)^{-1} \right]_{\gamma_1 \gamma_2}. \end{aligned} \quad (6)$$

This $\Sigma_H(z)$ contains all local spin-orbit and Coulomb correlation effects.

B. Self-consistency over charge density: Local Density Matrix Approximation

Instead of solving Eq. (3) directly, we look for an approximate solution including charge density self-consistency in a way which is similar to the well known rotationally invariant LDA+U method [16].

We start with calculating the HIA $\Sigma(z)$, Eq. (6), for given μ_H . In our applications, this starting μ_H corresponds to the nominal atomic f -shell occupation n_f . The initial solution for lattice electrons is represented by the LDA Green function matrix in the local basis $\{\phi_\gamma\}$,

$$\left[G_{LDA}(z) \right]_{\gamma_1\gamma_2} = \frac{1}{V_{\text{BZ}}} \int_{\text{BZ}} d\mathbf{k} \left[z + \mu - H_{LDA}(\mathbf{k}) \right]_{\gamma_1\gamma_2}^{-1}. \quad (7)$$

Note that the SOC is included in the LDA Hamiltonian $H_{LDA}(\mathbf{k})$. The local impurity Green function is calculated combining $\Sigma(z)$ and $G_{LDA}(z)$,

$$\left[G(z) \right]_{\gamma_1\gamma_2}^{-1} = \left[G_{LDA}(z) \right]_{\gamma_1\gamma_2}^{-1} - \left(\Delta\epsilon\delta_{\gamma_1\gamma_2} + \left[\Sigma_H(z) \right]_{\gamma_1\gamma_2} \right), \quad (8)$$

where $\Delta\epsilon$ is chosen to keep the given number of f -electrons n_f , and serves as an analogon of the difference between the impurity and the lattice chemical potentials [17].

With the aid of $G(z)$ from Eq. (8), the occupation matrix $n_{\gamma_1\gamma_2} = -\pi^{-1} \text{Im} \int^{E_F} dz [G(z)]_{\gamma_1\gamma_2}$ is evaluated, and used to construct the effective ‘‘LDA+U potential’’ [18], $V_U = \sum_{\gamma_1\gamma_2} |\phi_{\gamma_1}\rangle V_U^{\gamma_1\gamma_2} \langle\phi_{\gamma_2}|$, where

$$V_U^{\gamma_1\gamma_2} = \sum_{\gamma\gamma'} \left(\langle\gamma_2\gamma|V^{ee}|\gamma_1\gamma'\rangle - \langle\gamma_2\gamma|V^{ee}|\gamma'\gamma_1\rangle \right) n_{\gamma\gamma'} - V_{dc}\delta_{\gamma_1\gamma_2}. \quad (9)$$

In what follows, we have adopted the fully-localized (or atomic-like) limit (FLL) prescription of Solovyev *et al.* [20] for the double-counting term $V_{dc} = U(n_f - 1/2) - J(n_f - 1)/2$.

The set of Kohn-Sham-like equations is solved self-consistently over the charge density $\rho(\mathbf{r})$

$$\left(-\nabla^2 + V_{LDA}(\mathbf{r}) + V_U + \xi(\mathbf{l} \cdot \mathbf{s}) \right) \Phi_i(\mathbf{r}) = e_i \Phi_i(\mathbf{r}),$$

$$\rho(\mathbf{r}) = \sum_i^{\text{occ}} \Phi_i^\dagger(\mathbf{r}) \Phi_i(\mathbf{r}), \quad (10)$$

where the effective potential is the sum of the standard LDA potential $V_{LDA}(\mathbf{r})$ and the on-site electron-electron interaction potential V_U . Solving Eqs. (10) is similar to solving Eq. (3) in a sense that the selfenergy matrix $\Sigma(z)$ from Eq. (6) is substituted by the energy independent potential matrix defined in Eq. (9). After the self-consistency over the charge density is achieved, the LDA+U Green function matrix $G_U(z)$ in the local basis $\{\phi_\gamma\}$ is calculated from Eq. (7), substituting H_{LDA} by LDA+U Hamiltonian. Finally, new uncorrelated Green function

$$G_{LDA}(z) = \left[G_U^{-1}(z) + V_U(z) \right]^{-1} \quad (11)$$

is evaluated. The self-consistency loop is closed by inserting this new $G_{LDA}(z)$ into the matrix equation (8). In addition, an updated selfenergy $\Sigma(z)$ is calculated with the aid of Eqs. (5,6), where the new value of μ_H is set equal to the double-counting potential V_{dc} that corresponds to n_f obtained from the LDA+U Green function.

The condition $\mu_H = V_{dc}$ is essential and can be justified as follows. The double-counting term V_{dc} accounts approximately for the electron-electron interaction energy E_{LDA}^{ee} already included in the LDA. Namely, V_{dc} is a derivative of this mean energy contribution with respect to the f -shell occupation n_f , $V_{dc} = \partial E_{LDA}^{ee} / \partial n_f$. Indeed, it represents a mean-field value of the chemical potential μ_H that controls the number of f electrons.

The FLL [16, 20] choice of the double counting V_{dc} is not unique and other prescriptions, for instance the so-called ‘‘around-mean-field’’ V_{dc} [21, 22], can be used. Up to date, there is no precise solution for the double counting in the conventional LDA/GGA as it does not have a diagrammatic representation that would provide explicit identification of the corresponding many-body interaction terms. Therefore, ‘‘physical’’ arguments prevail in the choice of V_{dc} . Since we will be dealing with heavy actinides with well localized f -manifolds, it is reasonable to use the FLL double counting that is assumed to perform better for the case of f -occupation close to integer.

We will refer to our procedure as the ‘‘local density matrix approximation’’ (LDMA), since full convergence for G_{LDA} , $\rho(\mathbf{r})$ and μ_H is achieved when the local occupation matrix $n_{\gamma_1\gamma_2}$ is converged. We would like to emphasize that the self-consistency condition of equating the occupation matrix obtained from the local impurity Green function Eq. (8) to the local occupation matrix in solid (used in the LDA+U potential Eq. (10)) is a subset of general DMFT condition that the SIAM Green function is equal to the local Green function in a solid [23].

What makes our approach different from the conventional LDA+HIA given by Eq. (3) and from sim-

ilar basis set extension method of Ref. [24], is that we interchange the “inner” DMFT self-consistency loop over the bath Green function G_{LDA} , Eq. (11), and the “outer” self-consistency loop over the charge density $\rho(\mathbf{r})$, Eq. (10).

Up to now, our considerations did not depend on the choice of the basis set. The method becomes basis dependent, when a projector for the Bloch state $\Phi_i(\mathbf{r})$ solution of Eq. (10) on the local basis $\{\phi_\gamma\}$ is specified. The FP-LAPW method uses a basis set of plane waves that are matched onto a linear combination of all radial solutions (and their energy derivative) inside a sphere centered on each atom. In this case, we make use of the projector technique which is described in detail in Ref. [19]. It is important to mention that due to the full potential character care should be taken [18] to exclude the double-counting of the f -states non-spherical contributions to the LDA and LDA+U parts of potential in Eq. (10).

III. RESULTS

As representative systems to illustrate the LDMA numerical procedure, we select heavy actinides—Am, Cm and Bk. For all of them, the HIA is expected to provide a reasonable approximation for the selfenergy. We focus on comparison between the theory and available experimental results for valence-band photoelectron spectra (PES) as well as X-ray absorption (XAS) and electron energy-loss (EELS) spectroscopies. This comparison is often taken as important criterion of truthfulness of electronic structure calculations.

Experimental valence-band PES spectra will be compared with valence spectral densities resulting from the self-consistent LDMA. For the XAS and EELS experiments, we will compare the branching ratio B as well as strength of the spin-orbit coupling w^{110} for core-to-valence $4d-5f$ transition,

$$w^{110} = n_f^{7/2} - \frac{4}{3}n_f^{5/2},$$

$$\frac{w^{110}}{(14 - n_f)} - \Delta = -\frac{5}{2}\left(B - \frac{3}{5}\right), \quad (12)$$

where Δ represents a small correction term [11].

The actinides were calculated assuming paramagnetic state with fcc -crystal structure and the experimental volume per atom. The parameters of the local Hamiltonian, Eq. (4), were chosen as follows: $U = F_0 = 4.5$ eV, F_2 , F_4 and F_6 were taken from Table III of Ref. [11], and values of the SOC parameter ξ were extracted from LDA calculations ($\xi_{Am} = 0.35$ eV, $\xi_{Cm} = 0.36$ eV and $\xi_{Bk} = 0.42$ eV). The HIA Green function and selfenergy, Eqs. (5) and (6), were calculated along the real axis $z = \text{Re } z + i\delta$

with $\delta = 0.1$ eV. In the process, values 10 eV^{-1} and 100 eV^{-1} were used for the inverse temperature β . For self-consistency, 108 special k-points [25] in the irreducible 1/8th part of the BZ were used. The same sphere radius $R_{MT} = 3.1$ a.u. was used for all actinides, and $R_{MT} \times K_{max} = 10.70$ determined the basis set size. The f -manifold occupation n_f is varied in the calculations until the convergence better than 0.01 for n_f and 0.001 for all components of the on-site occupation matrix $n_{\gamma_1\gamma_2}$ is achieved. The charge density is fully converged to better than 10^{-5} e/a.u.^3 at each iteration.

We plot in Fig. 1 total and f -projected spectral densities resulting from self-consistent LDMA calculations (i. e., from converged Eq. (8)). In the case of Am, we obtain very good agreement with previous LDA+DMFT calculations [24, 26] as well as with our own non-self-consistent LDA+HIA calculations [7] for spectral peak positions in occupied and unoccupied parts of the spectrum. Comparison with the PES experimental data [27] is very good. No PES and BIS measurements exist for Cm and Bk metals. The results of present Cm calculations agree reasonably well with the results of recent DMFT study [6] supporting validity of the LDMA. We found practically no changes in the densities of states when β was decreased from 10 eV^{-1} to 100 eV^{-1} . The results turn out to be almost insensitive to the choice of β , since it enters explicitly only Eq. (5) and has practically no influence on the chemical potential μ_H .

For Am and Cm, the self-consistent value of n_f is very close to the atomic integer value (see Tab. I) in agreement with LDA+DMFT results [6, 24]. For Bk, deviation of n_f from the nominal atomic f^8 is somewhat bigger (Tab. I), suggesting a possibility of mixed-valence character in some of heavy actinides. In fact, Svane *et al.* [4] have already suggested mixed-valence states in Am, Cm and Bk on the basis of SIC-LSD calculations (see Tab. I of Ref. [4]) that split the f -electrons into localized manifold with fixed valence and an itinerant part. Present LDMA as well as previous LDA+DMFT [6, 24] calculations show that the tendency to mixed-valence in heavy actinides is substantially overestimated by the SIC-LSD theory.

Now we turn to comparison with XAS and EELS experiments [14]. In these experiments, the intensities $I_{5/2}$ ($4d_{5/2} \rightarrow 5f_{5/2,7/2}$) and $I_{3/2}$ ($4d_{3/2} \rightarrow 5f_{5/2}$) of the X-ray absorption lines are measured and the branching ratio $B = I_{5/2}/(I_{3/2} + I_{5/2})$ is obtained. Note that B is the only quantity which directly follows from the experiments. To extract the SOC strength w^{110} , the atomic sum rules are used in conjunction with the atomic calculations [11]. In order to compare with the experiment, we obtain $n_{5/2}$ and $n_{7/2}$ from the local occupation matrix $n_{\gamma_1\gamma_2}$ and make use of Eq. (12) to obtain B and w^{110} . We do not take into account the small correction factor Δ

[11].

The LDMA results for Am are shown in Table I in comparison with the experimental data [28] and the results of atomic intermediate-coupling (IC) calculations [29]. The LDMA calculated $n_{5/2}$, $n_{7/2}$, branching ratio B , and spin-orbit coupling strength are close to atomic IC and experimentally derived values. Once again, present calculations confirm localized nature of solid state Am f -manifold close to the atomic f^6 configuration.

The LDMA results for Cm are also shown in Table I in comparison with the results of DMFT calculations [6], atomic IC calculations [29] as well as with experimental data [14]. There is a very good agreement for $n_{5/2}$, $n_{7/2}$, B , and $w^{110}/(14 - n_f)$ between LDMA and atomic IC calculations. Also, the calculated branching ratio agrees with $B=0.75$ obtained from DMFT calculations [6]. Note that LDMA, DMFT and IC results agree with each other, and all slightly differ from experimentally observed B of 0.794 [14]. Gaining inspiration from LDA/GGA, Moore *et al.* [14] suggested that Cm $5f$ -states are shifted towards the LS coupling limit due to enhancement of the exchange interaction over the spin-orbit coupling. However, Shim *et al.* [30] noticed very recently that agreement between the theory and experiment for B improves substantially when the Slater integrals [11] are slightly reduced to account for the solid state screening.

To date, no XAS or EELS experimental data exist for Bk metal. The calculated $n_{5/2}$, $n_{7/2}$, branching ratio B , and spin-orbit coupling strength are listed in Table I together with the atomic IC f^8 calculations. The main difference between the solid state and the atomic f -manifolds is due to an increase in occupation of $n_{7/2}$ states. Nevertheless, the values of B and w^{110} per hole are practically the same. The measurements of the branching ratio are often used to obtain the experimental value of n_f . Our results illustrate that the knowledge of the B -ratio alone is not sufficient for precise determination of the f -manifold occupation.

Now we turn to an estimate of the effective local magnetic moment μ_{eff} in the paramagnetic phase. Importance of magnetism in Cm metal was emphasized recently in the context of its phase stability [13]. The temperature independent magnetic susceptibility is found for Am [31] that is consistent with zero μ_{eff} . The magnetic susceptibility measurements in the paramagnetic phase yield effective magnetic moment of $\sim 8 \mu_B$ for Cm and $\sim 9.8 \mu_B$ for Bk [31].

We can estimate semi-quantitatively the effective local moment making use of the atomic Hamiltonian, Eq. (4), and the chemical potential $\mu_H = V_{dc}$ that is self-consistently determined in the LDMA calculations. The expectation values of total, spin and orbital moment operators, \mathbf{J} , \mathbf{S} and \mathbf{L} , are calcu-

Am	n_f	$n_f^{5/2}$	$n_f^{7/2}$	B	w^{110}/n_h
LDMA ($\beta=10 \text{ eV}^{-1}$)	5.95	5.11	0.83	0.897	-0.743
LDMA ($\beta=100 \text{ eV}^{-1}$)	5.95	5.16	0.79	0.902	-0.756
atomic IC [11]	6	5.28	0.72	0.916	-0.79
Exp. [14]	6	5.38	0.62	0.930	-0.825
Cm	n_f	$n_f^{5/2}$	$n_f^{7/2}$	B	w^{110}/n_h
LDMA ($\beta=10 \text{ eV}^{-1}$)	7.07	4.04	3.03	0.736	-0.340
LDMA ($\beta=100 \text{ eV}^{-1}$)	7.07	4.04	3.03	0.737	-0.341
DMFT [6]	7.0	N/A	N/A	0.75	N/A
atomic IC [11]	7	4.10	2.90	0.75	-0.37
Exp. [14]	7	4.41	2.59	0.794	-0.485
Bk	n_f	$n_f^{5/2}$	$n_f^{7/2}$	B	w^{110}/n_h
LDMA ($\beta=10 \text{ eV}^{-1}$)	8.22	5.01	3.21	0.840	-0.591
LDMA ($\beta=100 \text{ eV}^{-1}$)	8.22	5.01	3.21	0.840	-0.601
atomic IC [11]	8	5.00	3.00	0.84	-0.61

TABLE I: Branching ratio B and spin-orbit coupling strength per hole w^{110}/n_h , where $n_h = (14 - n_f)$, for Am, Cm and Bk. Note that “experimental” values of $n_f^{5/2}$ and $n_f^{7/2}$ are not measured, but derived from sum rule Eq. (12) assuming integer atomic occupation n_f .

lated as grand-canonical averages,

$$\begin{aligned} \langle \mathbf{X}^2 \rangle &= \frac{1}{Z} \text{Tr} \left[\mathbf{X}^2 \exp(-\beta[H^{\text{at}} - \mu_H \hat{N}]) \right], \\ \mathbf{X} &= \mathbf{J}, \mathbf{S}, \mathbf{L}. \end{aligned} \quad (13)$$

Further, spin S , orbital L and total J moment “quantum numbers” are found using $\langle \mathbf{X}^2 \rangle = X(X+1)$ for $X = S, L, J$. Subsequently, the effective magnetic moment $\mu_{eff} = g_J \sqrt{J(J+1)}$ is evaluated, where the g-factor $g_J = (2S + L)/J$ is used.

For Am, we obtain $S = L = 2.33$ and $J = 0$ for $\beta = 100 \text{ eV}^{-1}$ in Eq. (13). Decreasing the value of β to 10 eV^{-1} yields a small difference in S and L values, and gives a non-zero value of $J = 0.099$. It means that the thermal population of the multiplets excited over the non-magnetic f^6 ground state starts to produce non-negligible contribution in Eq. (13).

For Cm, $S = 3.30$, $L = 0.40$, and $J = 3.50$ are calculated from Eq. (13) for $\beta = 100 \text{ eV}^{-1}$. Decrease of β to 10 eV^{-1} produces practically no difference in S , L , and J values. The corresponding local magnetic moment $\mu_{eff} = 7.94 \mu_B$ agrees well with atomic IC value and experimental data [31] (see Tab. II).

For Bk, Eq. (13) yields $S = 2.71$, $L = 0.40$, and $J = 6.00$ for $\beta = 100 \text{ eV}^{-1}$, as well as for $\beta = 10 \text{ eV}^{-1}$. The effective magnetic moment $\mu_{eff} = 9.8 \mu_B$ agrees well with the atomic f^8 IC value and experimental data [31] shown in Table II.

Our calculations, which are not bound by any particular atomic coupling scheme, illustrate once again that IC scheme is suitable for heavy actinides. Also, a good agreement of estimated μ_{eff} with experimental data is somewhat surprising.

$\mu_{eff}(\mu_B)$	Am	Cm	Bk
LDMA	0	7.94	9.54
IC [31]	0	7.6	9.3
Exp.[31]	0	~ 8	~ 9.8

TABLE II: Effective local magnetic moment μ_{eff} for Am, Cm and Bk. The atomic IC vales of μ_{eff} and experimental data [31] are shown.

IV. DISCUSSION AND CONCLUSIONS

For a better insight, it is useful to point out that in the current implementation, which is based on a single-site approximation, Eq. (8), to the solution of Eq. (3), the LDMA can be regarded as an extension of the LDA+U. Importantly, the on-site occupation matrix $n_{\gamma_1\gamma_2}$ is now evaluated in a many-body Hilbert space rather than in a single-particle Hilbert space as in the conventional LDA+U [16]. Current implementation can be further extended towards a fully self-consistent DMFT making use of Wannier-like basis set together with more sophisticated approximation for the quantum impurity solver along the lines proposed in Ref. [32].

Our approach to the charge self-consistency is essentially different from the one proposed by Lechermann *et al.* [33]. The on-site occupation matrix, instead of the full charge density, is obtained from the local Green function. The corresponding orbital-dependent effective potential is used in Eq. (10)

to calculate a new bath Green function G_{LDA} , Eq. (11), instead of orbital-independent Kohn-Sham (LDA/GGA) potential.

In this paper, we do not address the very important issues of the total energy calculation and determination of the equilibrium lattice properties. The practical implementation of accurate total energy calculations is ongoing work that will be discussed in detail in the future.

To summarize, we have presented a straightforward and numerically efficient local density matrix approximation (LDMA) to perform the LDA+HIA calculations in the FP-LAPW basis, including self-consistency over the charge density. This implementation is all-electron, incorporates spin-orbit interaction, and includes no shape approximations for the charge density. The method works well for the electronic spectrum of representative actinide Am, Cm and Bk metals. Importantly, the method allows fully self-consistent calculations for the paramagnetic phase of the local moment systems with strong Coulomb correlations. It can be extended to incorporate the total energy and to treat the magnetically ordered phases.

We are grateful to V. Drchal and V. Janiš for helpful comments and discussion. This work was supported by the Grant Agency of Czech Republic (Project 202/07/0644) and German-Czech collaboration program (436TSE113/53/0-1, GACR 202/07/J047).

-
- [1] S. Y. Savrasov, and G. Kotliar, Phys. Rev. Lett. **84**, 3670 (2000).
 - [2] A. B. Shick, V. Drchal, and L. Havela, Europhys. Lett. **69**, 588 (2005).
 - [3] D. Torumba, P. Novak, and S. Cottenier, Phys. Rev. B **77**, 155101 (2008).
 - [4] A. Svane, L. Petit, Z. Szotek, and W. M. Temmerman, Phys. Rev. B **76**, 115116 (2007).
 - [5] S.Y. Savrasov, G. Kotliar, and E. Abrahams, Nature **410**, 793 (2001).
 - [6] J. H. Shim, K. Haule, and G. Kotliar, Nature **446**, 513 (2007).
 - [7] A. Shick, J. Kolorenč, L. Havela, V. Drchal, and T. Gouder, Europhys. Lett. **17**, 17003 (2007).
 - [8] J.-X. Zhu, A. K. McMahan, M. D. Jones, T. Durakiewicz, J. J. Joyce, J. M. Wills, and R. C. Albers, Phys. Rev. B **76**, 245118 (2007).
 - [9] C. A. Marianetti, K. Haule, G. Kotliar, and M. J. Fluss, Phys. Rev. Lett. **101**, 056403 (2008).
 - [10] E. Wimmer, H. Krakauer, M. Weinert, and A. J. Freeman, Phys. Rev. B **24**, 864 (1981).
 - [11] K. T. Moore and G. van der Laan, Rev. Mod. Phys. **81**, 235 (2009).
 - [12] J.-C. Griveau, J. Rebizant, G. H. Lander, and G. Kotliar, Phys. Rev. Lett. **94**, 097002 (2005).
 - [13] S. Heathman, R. G. Haire, T. Le Bihan, A. Lindbaum, M. Idiri, P. Normile, S. Li, R. Ahuja, B. Johansson, and G. H. Lander, Science **309**, 110 (2005).
 - [14] K. T. Moore, G. van der Laan, R. G. Haire, M. A. Wall, A. J. Schwartz, and P. Söderlind, Phys. Rev. Lett. **98**, 236402 (2007).
 - [15] A. I. Liechtenstein and M. I. Katsnelson, Phys. Rev. B **57**, 6884 (1998).
 - [16] A. I. Liechtenstein, V. I. Anisimov, and J. Zaanen, Phys. Rev. B **52**, R5467 (1995).
 - [17] H. Kajueter and G. Kotliar, Phys. Rev. Lett. **77**, 131 (1996).
 - [18] A. B. Shick, V. Janiš, V. Drchal, and W. E. Pickett, Phys. Rev. B **70**, 134506 (2004).
 - [19] A. B. Shick, A. I. Liechtenstein, and W. E. Pickett, Phys. Rev. B **60**, 10763 (1999).
 - [20] I. V. Solovyev, P. H. Dederichs, and V. I. Anisimov, Phys. Rev. B **50**, 16861 (1994).
 - [21] V. I. Anisimov, J. Zaanen, and O. K. Andersen, Phys. Rev. B **44**, 943 (1991).
 - [22] J. Kuneš, V. I. Anisimov, A. V. Lukoyanov, and D. Vollhardt, Phys. Rev. B **75**, 165115 (2007).
 - [23] A. Georges, G. Kotliar, W. Krauth, and M. Rozenberg, Rev. Mod. Phys. **68**, 13 (1996).
 - [24] S. Y. Savrasov, K. Haule, and G. Kotliar, Phys. Rev.

- Lett. **96**, 036404 (2006).
- [25] H. J. Monkhorst and J. D. Pack, Phys. Rev. B. **13**, 5188 (1976).
- [26] A. Svane, Solid State Commun. **140**, 364 (2006).
- [27] J. R. Naegele, L. Manes, J. C. Spirlet, and W. Müller, Phys. Rev. Lett. **52**, 1834 (1984).
- [28] K. T. Moore, G. van der Laan, M. A. Wall, A. J. Schwartz, and R. G. Haire, Phys. Rev. B **76**, 073105 (2007).
- [29] Here we took the IC $n_{5/2}$, $n_{7/2}$ values given in Table IV of Ref. [11] and used Eq. (12) to calculate w^{110} and B .
- [30] J. H. Shim, K. Haule, and G. Kotliar, Europhys. Lett. **85**, 17007 (2009).
- [31] P. G. Huray and S. E. Nave, in Handbook on the Physics and Chemistry of the Actinides, Vol. 5, Freeman, A. J. and Lander, G. H., Eds. (Elsevier, Amsterdam) p. 311 (1987).
- [32] B. Amadon, F. Lechermann, A. Georges, F. Jollet, T. O. Wehling, and A. I. Lichtenstein, Phys. Rev. B **77**, 205112 (2008).
- [33] F. Lechermann, A. Georges, A. Poteryaev, S. Biermann, M. Posternak, A. Yamasaki, and O. K. Andersen, Phys. Rev. B **74**, 125120 (2006).

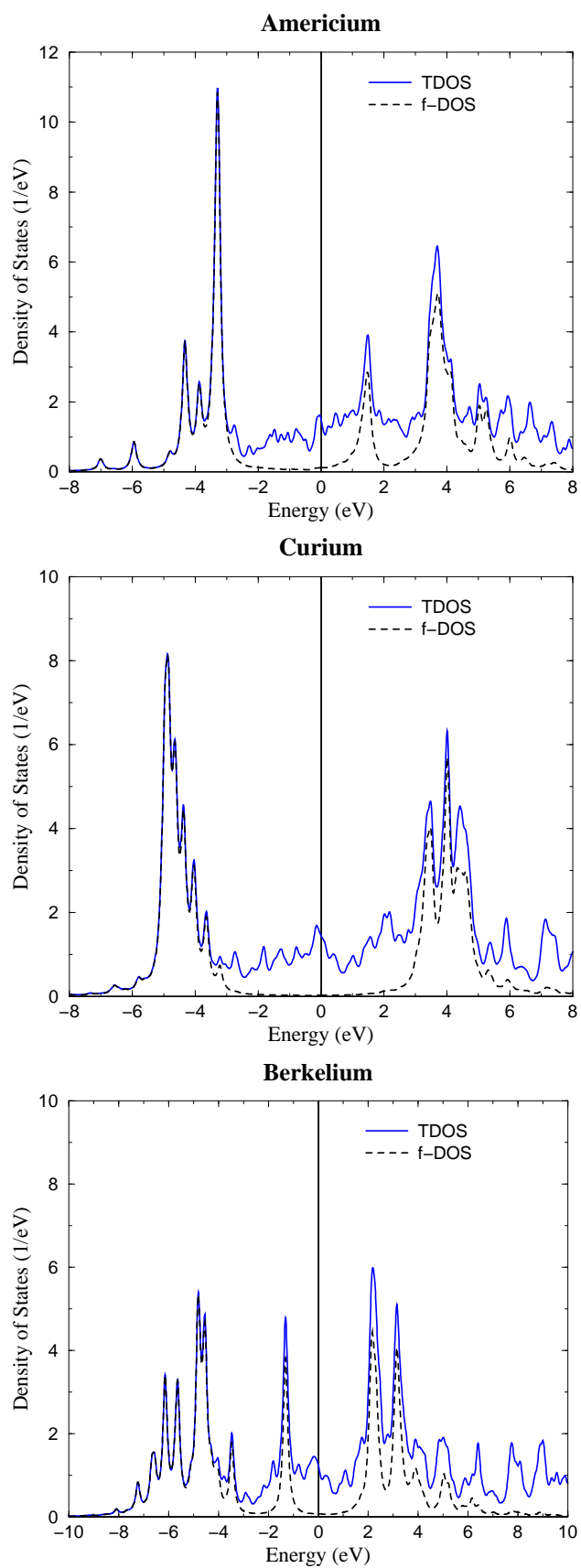


FIG. 1: Total-DOS and f -DOS for fcc -Am, fcc -Cm, and fcc -Bk for $\beta = 100 \text{ eV}^{-1}$.